Nuclear Instruments and Methods in Physics Research A 779 (2015) 25–32

Contents lists available at ScienceDirect

Nuclear Instruments and Methods in Physics Research A

journal homepage: www.elsevier.com/locate/nima

High-efficiency microstructured semiconductor neutron detectors for direct ^{3}He replacement

R.G. Fronk [a,*], S.L. Bellinger [a], L.C. Henson [a], D.E. Huddleston [b], T.R. Ochs [a], T.J. Sobering [b], D.S. McGregor [a]

[a] S.M.A.R.T. Laboratory, Department of Mechanical and Nuclear Engineering, Kansas State University, Manhattan, KS 66506, USA
[b] Electronics Design Laboratory, Kansas State University, Manhattan, KS 66506, USA

ARTICLE INFO

Article history:
Received 14 October 2014
Received in revised form
11 December 2014
Accepted 9 January 2015
Available online 17 January 2015

Keywords:
MSND
Helium-3 replacement
Neutron detector

ABSTRACT

High-efficiency Microstructured Semiconductor Neutron Detectors (MSNDs) have been tiled and arranged in a cylindrical form factor in order to serve as a direct replacement to aging and increasingly expensive ^{3}He gas-filled proportional neutron detectors. Two 6-in long by 2-in diameter cylinders were constructed and populated with MSNDs which were then directly compared to a 4 atm Reuter Stokes ^{3}He detector of the same dimensions. The Generation 1 MSND-based ^{3}Helium-Replacement (HeRep Mk I) device contained sixty-four 1-cm^2 active-area MSNDs, each with an intrinsic neutron detection efficiency of approximately 7%. A Generation 2 device (the HeRep Mk II) was populated with thirty 4-cm^2 active-area MSNDs, with an intrinsic thermal neutron detection efficiency of approximately 30%. The MSNDs of each HeRep were integrated to count as a single device. The ^{3}He proportional counter and the HeRep devices were tested while encased in a cylinder of high-density polyethylene measuring a total of 6-in by 9-in. The ^{3}He counter and the HeRep Mk II were each placed 1 m from a 54-ng ^{252}Cf source and tested for efficiency. The ^{3}He proportional counter had a net count rate of 17.13 ± 0.10 cps at 1 m. The HeRep Mk II device had a net count rate of 17.60 ± 0.10 cps, amounting to $102.71 \pm 2.65\%$ of the ^{3}He gas counter while inside of the moderator. Outside of moderator, the ^{3}He tube had a count rate of 3.35 ± 0.05 cps and the HeRep Mk II device reported 3.19 ± 05, amounting to $95.15 \pm 9.04\%$ of the ^{3}He neutron detector.

1. Introduction

The high cost and waning availability of ^{3}He gas has been steadily increasing the expense of detectors that are based on this rare gas. ^{3}He proportional neutron counters are widely used for neutron detectors of various sizes, including large-area portal monitors down to portable handheld REM meters, all of which are typically operated in the presence of gamma-ray background that must be suppressed. The recent push for replacements for these ^{3}He-based detector technologies has motivated much of the research dedicated to the development of high-efficiency, low-cost, low-power Microstructured Semiconductor Neutron Detector (MSND)-based ^{3}He-Replacement (HeRep) detectors, shown in Fig. 1. Semiconductor with a thin-film coating of neutron reactive material deposited on a planar rectifying diode have been investigated for the past few decades as a potential neutron detector technology while maintaining high gamma-ray rejection characteristics [1–3]. MSNDs were developed as a means of increasing the relatively low efficiency of the planar thin-film-coated devices (typically < 4–5% intrinsic) up to their theoretical maximums above 40% intrinsic detection efficiency for single 0.5-mm thick devices [4–16] while maintaining gamma-ray rejection ratios (GRR) of 10^{-6} or better [12]. The increase in intrinsic neutron detection efficiency stems from the two primary benefits of perforating a semiconductor diode; increased neutron absorption and increased probability of interaction of the charged neutron reaction products in the semiconductor diode. Furthermore, stacking two common thin-film devices will not double the detection efficiency over a single device, a consequence of reaction product self-absorption. However, offset-stacking two MSNDs can double the detection efficiency, primarily due to the elimination of the neutron streaming paths in the semiconductor sidewalls [17–19]. MSNDs can be mass produced using inexpensive silicon VLSI processing techniques and readily-available ^{6}LiF neutron conversion material, among other conversion materials. The mass production capability and modularity of the MSND allows for many MSNDs to be arranged in the ^{3}He-tube form factor, amongst other form factors [20–25]. Hundreds of MSNDs can be produced using batch-processing methods in a single run, each with nearly identical neutron detection properties.

* Corresponding author. Tel.: +1 785 532 6128.
E-mail address: rfronk@ksu.edu (R.G. Fronk).
URL: http://www.mne.ksu.edu/research/centers/SMARTlab (R.G. Fronk).

http://dx.doi.org/10.1016/j.nima.2015.01.041
0168-9002/

Fig. 1. Depicted is a side-by-side comparison of a 6-in. long by 2-in. diameter ^{3}He Reuter Stokes proportional counter pressurized to 4 atm, shown on the left in each image, and the 6 in. by 2 in. HeRep device on the right in each image.

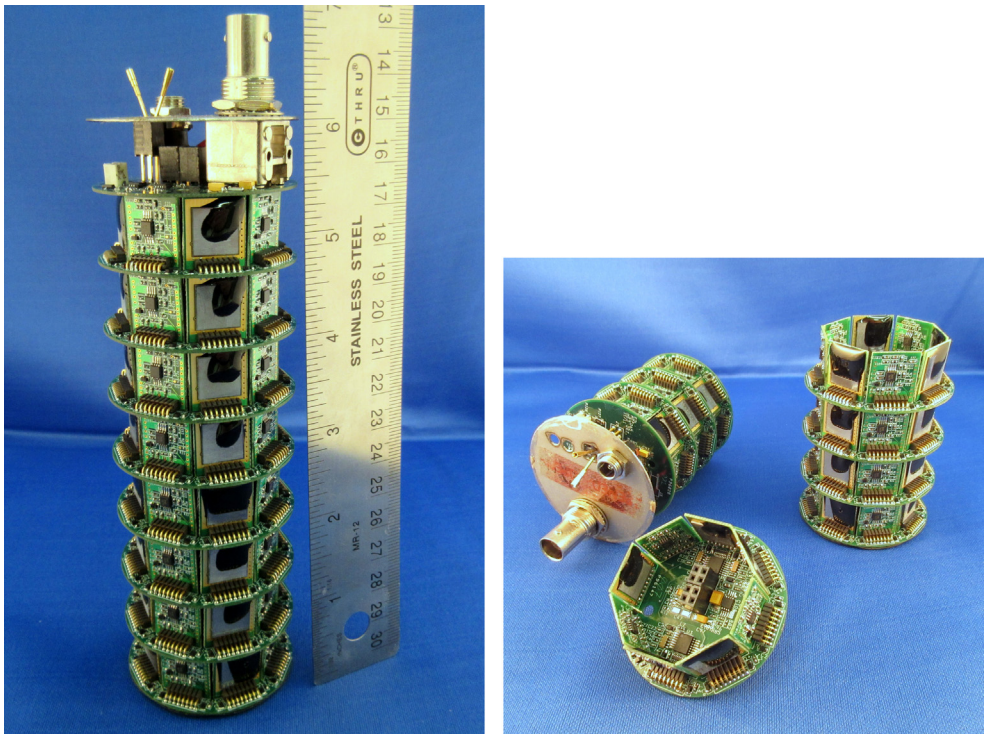

Fig. 2. Depicted (left) is the fully assembled HeRep Mk I device designed to directly replace a standard ^{3}He tube and (right) is the HeRep Mk I that has been separated, displaying the layout of one of its stackable layers.

The first-generation Helium Replacement device (HeRep Mk I) was designed as eight 1-cm^2 active-area MSNDs arranged concentrically around a HDPE puck, designed to stack and form a right circular cylinder, as shown in Fig. 2. In one permutation, eight of these pucks were then stacked end-to-end to form a 6-in. long by 2-in. diameter cylindrical neutron detector. The number of pucks used in the device can be varied in order to obtain different tube heights. Furthermore, the system can be re-designed with fewer MSNDs around the parameter of the tube in order to reduce the overall diameter of the device, allowing the HeRep to replace ^{3}He-based detectors of various dimensions. The second-generation Helium Replacement device (HeRep Mk II) was designed with thirty 4-cm^2 MSNDs tiled into strips, which were then arranged cylindrically, as shown in Fig. 3. Five of the 4-cm^2 MSNDs were mounted to each strip. Six strips were then arranged into a cylindrical fashion, designated the 'Hexastrip pattern', as shown in Fig. 4. The modular nature of these detector designs allows for either device to be scaled to fit any cylindrical form factor.

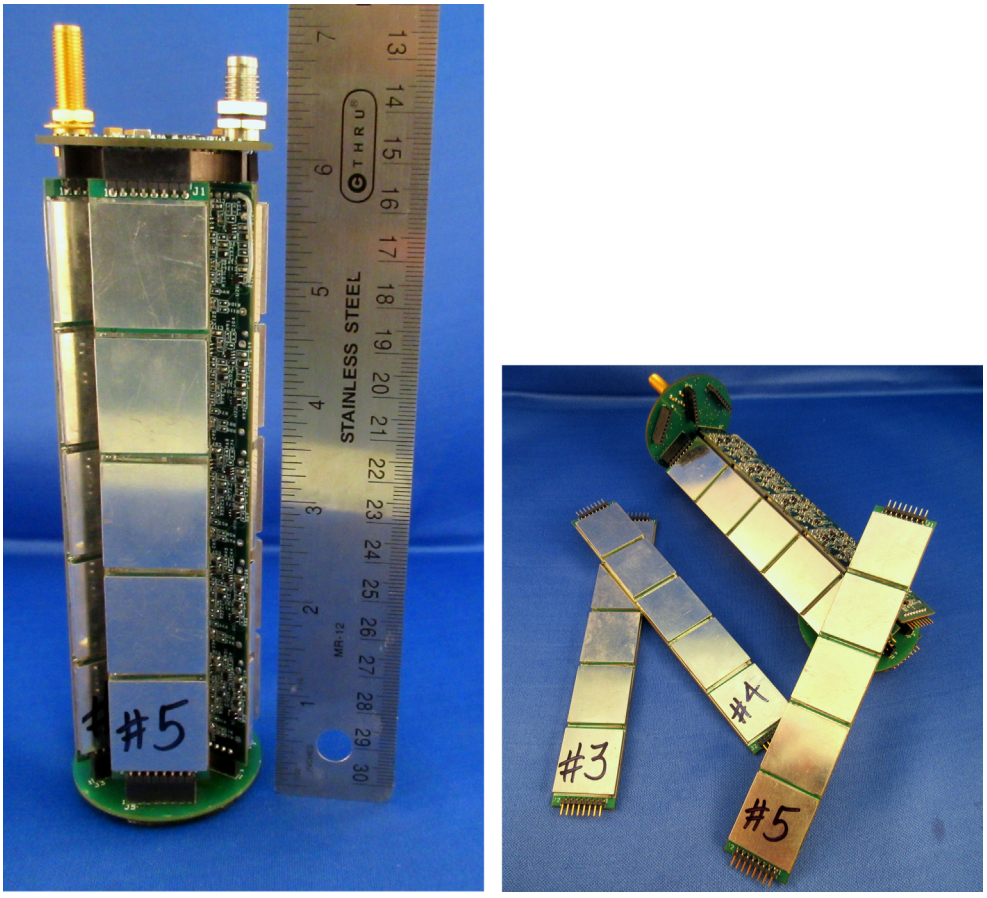

Fig. 3. Depicted (left) is the HeRep Mk II, fully assembled, designed to improve upon the HeRep Mk I and replace ^{3}He-based detectors and (right) the strips of MSNDs have been removed for display. The strips are numbered for reference during testing.

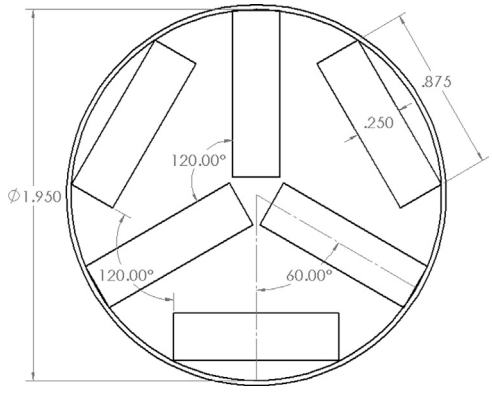

Fig. 4. MSNDs are arranged in a circular-Hexastrip pattern in the HeRep Mk II to eliminate neutron streaming. Neutrons that are able to stream through the sidewalls of an MSND will be incident on a second MSND at a non-normal angle.

Furthermore, the solid-state nature of these detector elements and their electronics allows for HDPE moderator to be contained within the detector cavity, a construction that is not possible for ^{3}He or other gas-filled counters.

2. Design

2.1. MSND design

The main component of both HeRep versions are MSNDs. These semiconductor-based neutron detectors have been researched over the past decade as replacement detectors for planar-type devices. The functional MSND design includes a semiconductor etched with trenches, subsequently backfilled with a neutron conversion material, and offers a ten-fold increase in detection efficiency over their planar counterparts [6]. A neutron incident upon the detector can be absorbed by the conversion material, inducing fission, and produce a pair of charged-particle reaction products. The reaction-product particle types and energies are characteristics of the conversion material. For thermal (slow) neutrons and conversion materials based on B or Li, these reaction products are emitted in opposite directions. As the ionized reaction products travel through the detector materials, they produce ionization through Coulombic interactions. Electrons that are excited into the conduction band of the semiconductor are swept out through an applied voltage bias, thereby, generating a signal pulse.

There were two designs for MSNDs used to populate the HeRep Mk I and Mk II. The HeRep Mk I was populated with straight-trenched, 1-cm^2 active area MSNDs etched to a depth of 175 μm. These MSNDs typically yielded an intrinsic thermal neutron detection efficiency of 5–10% with an LLD setting such that electronic noise and gamma-ray sensitivity were sufficiently reduced. The HeRep Mk II was populated with 4-cm^2 active area MSNDs etched with straight trenches to a depth of 400 μm, shown in Fig. 5. The 4-cm^2 MSNDs were patterned with 20-μm-wide trenches and a 40-μm pitch. With this trench layout, and greatly improved fabrication techniques, the MSNDs typically have an intrinsic thermal neutron detection efficiency of 25–30%, as calibrated with a ^{3}He proportional detector with a thermalized and diffracted neutron beam; measurement method and details described in the literature [26]. The MSNDs were calibrated in the 0.5 mm-diameter thermal neutron beam such that

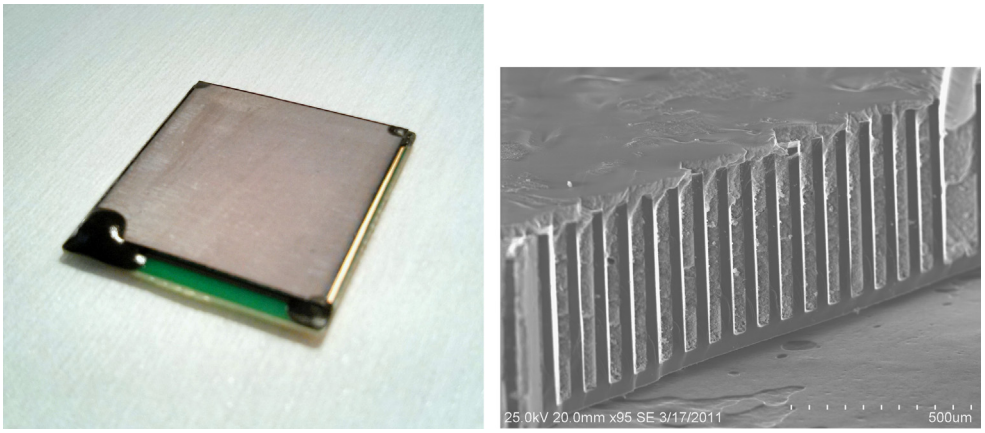

Fig. 5. (left) Depicted is a finished 2 cm by 2 cm MSND that was used to populate the HeRep neutron detector device and (right) a cleaved-SEM image of said MSND, backfilled with ^{6}LiF neutron conversion material. A total of 30 of these MSNDs were used in the HeRep Mk II.

the beam was normal to, and completely incident upon, each of the MSNDs. The count rate of each MSND tested was compared to that of a calibrated ^{3}He proportional counter, whereby the MSND detector efficiency was determined [26].

2.2. ^{3}Helium replacement design

^{3}He gas has a relatively large microscopic thermal neutron absorption cross sections (5330 b for 2200 m s^{-1} neutrons) which contributes to intrinsic detection efficiencies often exceeding 80% for a 2-in. diameter, 4-atm tube [26]. Unfortunately, this detection efficiency is not uniform across the entire face of the detector. Dead regions at each end of the gas tube, a consequence of insulating standoffs and field tubes, do not contribute to detection efficiency, and thus reduce the active area of the tube by up to ~30% for a handheld-sized unit. Similarly, the 80% intrinsic efficiency is only valid for neutrons intersecting the center of the detector tube, a fact often neglected in reports. The MSND-based HeRep does not suffer from these intrinsic problems. MSNDs populate the entire length of the tube, thereby, increasing the total area of the detector that is sensitive to neutrons. Shown in Fig. 4 is the MSND arrangement of the HeRep Mk II neutron detector. The only streaming paths through in the HeRep Mk II neutron detector is between the MSNDs on each string. However, the inner void of the device can be filled with HDPE moderator, which can then act to scatter streaming neutrons. The addition of moderator inside of the detector can also help improve the fast neutron response of the HeRep detector. For both the HeRep Mk I and the HeRep Mk II device, the MSNDs were arranged in a cylindrical format such that the detector could act as a direct replacement for ^{3}He gas-filled neutron detectors. Further, the cylindrical format allowed for direct comparisons to conventional ^{3}He-based neutron proportional counters of the same size.

2.3. Detector simulation

MCNP6 was used to construct a model of the HeRep Mk II in order to optimize the MSND arrangement. MSNDs etched with 400-μm-deep trenches and a 40-μm unit cell pitch, where the trench widths were 20 μm, were used in the virtual HeRep model. Upon absorption of a thermal neutron, the MCNP6 simulation generates charged-particle reaction products within the modeled conversion material. These charged particles are tracked by MCNP6 as they traverse the trenches and semiconductor sidewalls. Energy deposited into the Si semiconductor substrate and Si sidewalls is recorded and added to a tally. The intrinsic thermal neutron detection efficiencies of the MSNDs modeled and simulated in this fashion matched well with previously reported results for detectors

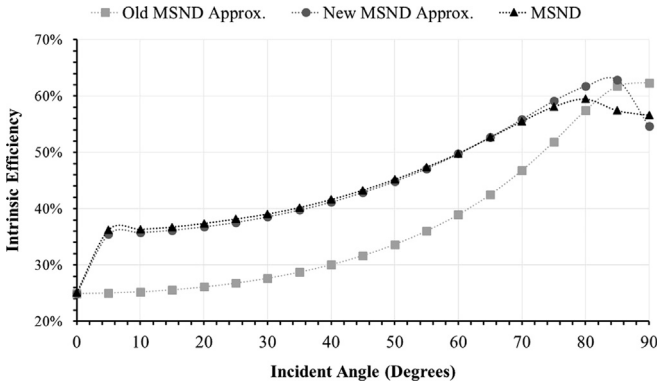

Fig. 6. Depicted is plot developed to show device efficiency when irradiated with a small beam of thermal neutrons at an polar-varying angle. MCNP6 was used to simulate an MSND with charged-particle tracking turned on (labeled MSND) and an approximate model that uses nearly three orders of magnitude less computing time without tracking charged reaction products (labeled Old and New MSND Approximation).

of this same geometry modeled for an LLD setting of 300 keV [6]. However, due to the computationally-expensive charged-particle tracking, a simplified model of the MSND was developed to simulate the response of the HeRep. A method of simplifying the MSNDs to a single, homogenous volume was reported in the literature [27]. In the citation [27], a tally multiplier card was used to convert a percentage of the neutron absorptions occurring in the volume into a 'count.' However, the described method introduces inaccuracies in the modeled outcome for detection efficiency as the neutron current incident angle varies from normal. A new MSND approximation model was therefore developed to better suit the purpose of the HeRep model with accurate results, as neutrons could enter into the device at varying angles.

The new MSND approximation model includes trenches and sidewalls in the detector architecture, giving rise to streaming paths that are present in actual devices, but not included in the aforementioned single-homogeneous volume (SHV) model. To test the new MSND approximation model, the incident angle of a 0.5-mm diameter thermal neutron beam was varied from 0° to 90° with respect to the normal face of the detector. This process was also applied to the rigorous charged-particle-tracking (CPT) model, thereby, allowing for a direct comparison of the results. The improved method for approximating the MSNDs shows good angular tracking of the intrinsic detection efficiency, unlike the original single-volume approximation, as revealed in Fig. 6. A typical MSND can have an intrinsic detection efficiency increase of nearly 50% by simply rotating the thermal neutron beam about the detector over a

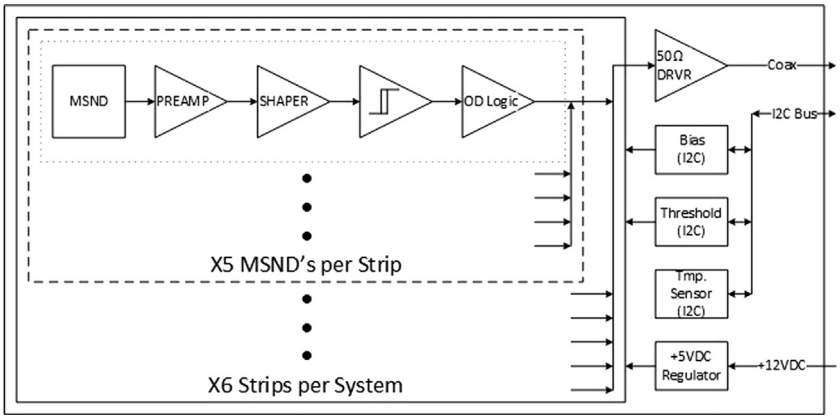

Fig. 7. Depicted is a functional block diagram for the 3HE Replacement electronics. Each channel consists of the MSND preamplifier/Shaper/discriminator chain. A common detector bias and discriminator threshold are applied to all channels. The outputs of the discriminators are "wired-OR" summed to provide an aggregate pulse for counting neutron events. This signal is applied to a 50 Ω cable driver. The detector bias and discriminator threshold are set using non-volatile digital potentiometers on an I2C bus. There is also an internal temperature sensor read out over I2C.

10° variation from normal, and the efficiency can more than double as the beam is swept towards 90°. Only a small difference in response was observed between the new model and the rigorous CPT model, as evidenced in Fig. 6, whereas a considerable difference is evidence between the new model and the SHV model.

The small variation between the new model and the CPT model can be attributed to differences in the modeling assumptions for neutron absorption. In the new model, the assumption is that neutrons enter perpendicular to the ^{6}LiF backfilled trenches, thereby, being attenuated exponentially with respect to their depth in the trench. Because some reaction products can entirely escape the detector if generated near the surface, the probability of these reaction products intersecting the semiconductor and being detected increases as neutrons are absorbed deeper in the trench. The new model sets this absorption probability as a function of depth in the trench. However, in reality, as the neutron beam is rotated about the MSND, neutrons will cross both ^{6}LiF backfilled trenches and Si fins. Consequently, fewer neutrons are absorbed near the device surface, resulting in fewer escapes. Hence, the neutron absorption depth must be adjusted to compensate for the Si regions, which is accomplished by the CPT model but not the new approximation model. This effect is most pronounced for a beam rotation between 75°–90° beam rotation, as shown in Fig. 6.

Using the new model, MSNDs were each designed with a repeating trench-sidewall lattice structure inside of a unit-cell 'universe' which was then repeated inside of a diode 'universe'. The MSNDs themselves were then repeated along each of the detector strips. Afterwards, these strips were repeated rotationally to form the HeRep Mk II design pattern. The HeRep Mk II MCNP model was set in an open room with concrete walls. The dimensions and major features of modeled room closely resembled the room in which the real-world measurements took place. A bare Cf-252 point source was placed one meter from the axial center of the HeRep detector. The HeRep detector was modeled 1 m from the concrete floor and the source was 1.075 m from the floor. The source was allowed to emit in all directions to allow for proper modeling of room-scatter contribution. A ^{3}He model was created to directly compare to the HeRep device. A 6-in. long by 2-in. diameter ^{3}He tube was modeled at 4 atm to mimic the aforementioned 'real-world' Reuter Stokes ^{3}He tube. The virtual ^{3}He detector model also included the regions on the ends that were not sensitive to charge collection. An F6 and F8 tally card were used to determine the ^{3}He detector response to a ^{252}Cf source with an activity of 125,000 n s^{-1}. The ^{3}He model response rate was determined to be within $1.51 \pm 0.03\%$ of the measured real-world ^{3}He count rate. The simulation was then repeated for the HeRep device which was found to have $101.03 \pm 2.52\%$ of the measured real-world HeRep count rate and $105.36 \pm 3.99\%$ of the simulated ^{3}He tube response. The discrepancy between the model and the real-world measurement likely lies in the assumption that at an LLD of 150 keV, each MSND's intrinsic thermal neutron efficiency is 32%. However, variations in leakage current and capacitance likely drops these efficiencies slightly. It was concluded that the HeRep device model was adequate for the optimization of future detector designs.

2.4. Electronics design

The electronics supporting the HeRep devices were designed by the Electronics Design Laboratory (EDL) at Kansas State University. The two primary goals for the HeRep electronics design were: 1) low power usage, and 2) total internal signal processing with a 5 V TTL-pulse output. With these two design goals in mind, a compact, standalone hybrid MSND device package was developed.

Each of the thirty MSNDs in the HeRep MkII is accompanied by its own pre-amplifier, amplifier, and discriminator electronics. When charge is excited in the MSND from the Coulombic interactions of the charged reaction products, the reverse bias (set between 0–2.7 V) sweeps the charge out of the MSND diode. The preamplifier integrates the charge collected, typically between 30 and 1800 fC, generating a voltage pulse with a gain of 0.36 mV/fC. The pulse is shaped using a 10 μs shaping time with an overall shaper gain of 27.4 V/V. The overall gain of the system is 9.85 mV/fC. The amplified signal is then sent to the onboard discriminator which, if above the lower-level discriminator, will be passed as a 5 V low-voltage complementary metal oxide semiconductor (LVCMOS) pulse that is approximately equal to the time above threshold. For the purposes of the device characterization, an output driver was implemented so that the LVCMOS signal could be driven into a 50 Ω-terminated input on a NIM bin counter/timer[1] (Fig. 7).

The entire device is powered using a standard 12 V AC-to-DC power adapter rated at 500 mA, available as an off-the-shelf component. Though the HeRep draws only 30 mA at idle, the TTL-pulse generator draws an additional 100 mA during high neutron-count rates. The power cable doubles as the I2C signal input for the programmable bias and LLD settings. The bias and LLD are both separately programmable through an accompanying program box that couples with the HeRep detector onboard bias and LLD programmable potentiometers, as shown in Fig. 8. The LLD can be programmed from 0 to 1 V, in reference to the output signal from

[1] An Ortec model 871 was used in the present work.

Fig. 8. Depicted is the program box designated for the HeRep device. The program box is used to program the bias applied to the MSNDs and lower-level discriminator settings for the TTL-pulse generator. Setting are varied from 0 V to −5 V applied bias and 0–1 V threshold voltage in 256 increments, 0.02 V and 0.004 V per increment respectively. The program box also monitors the HeRep's internal temperature. The box can be removed from the system once the bias and threshold have been programmed.

the shaper/amplifier, through the accompanying programmer box. The reverse bias on the detectors is variable from 0 to 5 V and is programmed in the same fashion as the LLD. LLD and bias settings are somewhat dependent on environmental variables (such as temperature) due to increasing leakage current and capacitance of the MSND, rather than changes to the electronics package. Presently, MSND-electronics pairs have been tested for functionality up to 50 °C to little detriment. In the case of the HeRep Mk I and Mk II, LLD and bias settings are limited to the 'worst' MSND present within the device. Further studies will be conducted to fully characterize the functionality of the HeRep as a whole with respect to environmental variables. Once the settings are programmed into the digital potentiometers, the programmer box can be disconnected and the He-Rep operates as a standalone device.

3. Fabrication

3.1. MSND fabrication

Thirty 4-cm^2 MSNDs were used to populate the HeRep Mk II neutron detector[2], shown in Fig. 6. MSNDs were fabricated using 30 kΩ-cm, [1 1 0]-oriented, 500 μm-thick silicon wafers with the primary flat cut on the (1 1 1) plane. This high-purity silicon allows for long carrier lifetimes on the order of milliseconds. A wet thermal oxide was grown on the surface of the silicon to a thickness of 2.75 μm. The surface to be etched was patterned using a positive photoresist with the trench pattern carefully aligned to the (1 1 1) plane. The trench pattern was then etched into the SiO_2 layer with a dilute-HF etch, exposing the silicon under the SiO_2 layer. Next, a diffusion window pattern was etched into the remaining oxide. A thin layer of oxide remained so as to act as an etch mask against the potassium hydroxide (KOH) etch but was thin enough as to also allow for the device's active area to be cleared of SiO_2 for a latter diffusion process. The wafers were submerged into a heated bath of KOH to etch the perforations into the silicon. Once an etch depth of 400 μm was achieved, the wafers were removed and rinsed. The remaining oxide etch mask was removed using dilute-HF, exposing the diffusion window, and the wafer was then cleaned with a typical RCA clean. Boron was diffused into the top surface of the etched side of the wafer using a BN solid-source diffusion process, thereby, forming the *pn*-junction blocking contact. The final dopant concentration resulting in a conductive layer that provided even distribution of the applied bias while not contributing significantly to the surface recombination leakage current. Finally, a Ti/Al/Ti/Au backside ohmic contact was evaporated onto the wafer.

The wafer was backfilled with nano-sized ^{6}LiF using centrifugal material deposition [12]. ^{6}LiF was produced by titration of ^{6}LiOH with HF. ^{6}LiF powder produced in this manner typically yields cubic particles with sizes between 1–40 μm-wide. The ^{6}LiF powder was nano-sized with a thermal condensation method and suspended into a colloid solution [19,28]. The etched wafer was placed at the bottom of the solution and the whole system was centrifuged for several minutes with at an acceleration of several hundred *g*-force, cleanly and evenly backfilling the trenches with neutron reactive material, as shown in Fig. 6. The MSNDs were then diced from the wafer and tested for their leakage current characteristics. MSNDs are either accepted or rejected based on their leakage current and capacitance measurements. Presently, MSNDs can be accepted if the total leakage current is less than 100 nA (25 nA cm^{-2}) and the capacitance is below 700 pF, otherwise the detector electronics will not properly couple with the MSND. Twelve MSNDs, each 4 cm^2 area, can be fabricated upon a single 4-inch diameter silicon wafer, and up to fifty such Si wafers can be processed simultaneously within the S.M.A.R.T. Laboratory microelecronics facility. MSND sensor yield per wafer is typically 80–100%. MSND leakage currents average 1–5 nA cm^{-2} with capacitances of ~600 pF and ~100 pF at 1 kHz and 1 MHz measuring frequency, respectively, when operated with a 1 V reverse bias[3].

3.2. Detector electronics

MSNDs are mounted to their electronics using an in-house designed Disposable Detector Board (DDB), which is in turn mounted to the detector string electronics board. The DDB is a four-contact solder-bumped mount that is designed to be simple to manufacture and with low cost. The MSND is mounted to the DDB using EPO-TEK H20E, a two-part conducting silver epoxy. The MSND is then wire bonded to the signal pad with a 1 mil Al/Si wire approximately 1 mm in length. The wirebond is protected with black 3 M DP-270, an inert two-part insulating epoxy that also works to block light. The bias, preamplifier, shaper, amplifier, threshold, and discriminator electronics are mounted to the detector string electronics board opposite the detector mounting location. The DDB mounts to the pre-amplifier/amplifier and discriminator board, effectively coupling the MSND to its electronics. The MSNDs are mounted in a string formation on daughter boards, as shown in Fig. 3. The strings allow for the signal from devices further down the string to pass around devices higher in the detector string without signal crosstalk. The LVCMOS outputs from each detector are "summed" using a wired "OR" connection of open-drain gates. A single pull-up is implemented on the motherboard for the string outputs. The motherboard contains all electronics necessary to drive the LVCMOS signal into a 50Ω impedance input through up to 15 m of BNC R58 cable. The motherboard also contains non-volatile digital potentiometers for setting and maintaining the system applied bias and threshold settings.

3.3. Moderator and cylindrical design

Most ^{3}He proportional counters are of a cylindrical design with varying lengths and diameters. The cylindrical shape of the detector is

[2] Sixty-four MSNDs were used for the HeRep Mk I, each only 1 cm^2 area.

[3] The MSNDs used in the HeRep Mk I were fabricated in the same manner as those used in the HeRep Mk II, but each with 1 cm^2 area fabricated in 10 kΩ-cm silicon.

Table 1
HeRep vs. ^{3}He-proportional counter with moderator

Detector	Measurement	Time (s)	Counts
HeRep	Cf-252	1800	32,710
HeRep	Background	1800	1,034
^{3}He Prop. Ctr.	Cf-252	1800	31,143
^{3}He Prop. Ctr.	Background	1800	302

Table 2
HeRep vs. ^{3}He-proportional counter without moderator

Detector	Measurement	Time (s)	Counts
HeRep	Cf-252	1800	6,872
HeRep	Background	1800	1,139
^{3}He Prop. Ctr.	Cf-252	1800	6,483
^{3}He Prop. Ctr.	Background	1800	458

useful in utilizing a 1/r electric field density, better promoting electron avalanching near the anode. The cylindrical symmetry also promotes uniform detector response around the angular (θ) coordinate. The overall goal of the HeRep MSND-based device is to directly replace ^{3}He proportional counters in existing systems, therefore, the HeRep was also designed with a cylindrical shape.

The overall length of the HeRep device is determined by the length of the detector string, and thus, the number of MSNDs used to populate the string. Six MSNDs were strung together for the current generation HeRep forming a sting that is just under 6 in. in length. A 2-inch diameter Reuter Stokes ^{3}He proportional counter was used for the detector comparison; thus a 2-inch diameter motherboard was created to mount and sum the detector strings. MCNP modeling has indicated that detector efficiency is roughly proportional to the number of MSNDs present within the detector system. The Hexastrip detector layout was chosen as it accomplished two primary goals; the layout offered a maximum detector density while maintaining system symmetry, as shown in Fig. 4.

4. Testing

Testing was performed with and without a high-density polyethylene (HDPE) moderator surrounding the detector. MCNP simulations indicated that a HDPE cylinder with a 2-inch hole through the center, when exposed to a ^{252}Cf neutron source, has an optimal outer diameter 6 in., thereby, providing a 2 in. thick HDPE moderator around the cylindrical detectors. Two HDPE cases were built, designed from the MCNP model, one for the Reuter Stokes ^{3}He gas-filled proportional counter and another identical case for the HeRep detectors. The HDPE cylinder, when fitted with a handle, also served as a means of carrying and protecting the detectors. During the measurements, the ^{3}He proportional counter was operated at a bias of 1300 V and 2 μs shaping time.

The two detectors were tested separately in a largely open room under identical conditions. The LLD for the HeRep device was set to approximately 150 keV. The tests were conducted in the same building as the KSU TRIGA MkII research nuclear reactors; hence tests and background measurements were conducted between periods of reactor operation. The detectors were placed approximately 1 m above a concrete floor and at least 2 m from the operator. A bare 54 ng ^{252}Cf source, with a neutron emission rate of approximately 125,000 n s^{-1}, was positioned at center of the detectors, perpendicular to the long axis, at a distance of 1 m. Measurements were performed in 1800 s intervals, the results for which are listed in Table 1. The detectors were then removed from their HDPE moderator shells and retested under the exact same conditions without moderator, in the results of which are listed in Table 2.

Afterwards, the HeRep device was tested for angular dependence. The HeRep was reinserted into the HDPE moderator cylinder at a distance of 1 m from the bare ^{252}Cf source, similar as in previous measurements. After the first measurement, the detector was rotated 15° and a new measurement was conducted. The detector was again rotated through 15° increments for each measurement, and the process was repeated until the detector had undergone a full rotation. Shown in Fig. 9 is the variation in the count rate of the detector as a function of irradiation angle, which never varied more than 3.80% from the mean count rate. A more rudimentary measurement was taken with the HeRep outside of the moderator cylinder. Two measurements were performed, one with the ^{252}Cf source normal to an MSND strip inside the detector chamber and another measurement with the HeRep rotated by 60°. The measurement revealed a reduction in count rate of approximately 1.7%.

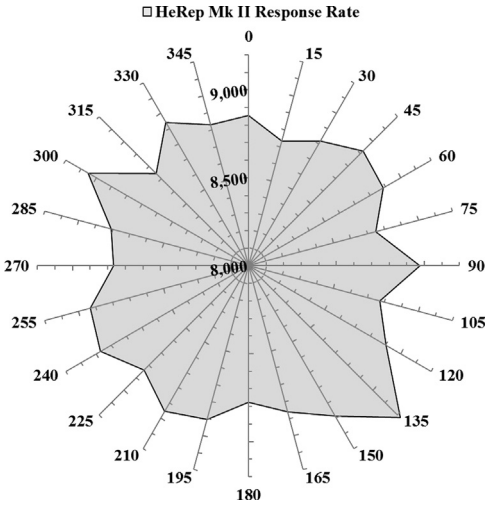

Fig. 9. Depicted is the angularly-dependent measurements of the HeRep device inside of a 2-in. cylinder of HDPE. The detector was placed 1 m from a 54 ng Cf-252 source. The device was rotated 15° after each measurement until it had been rotated completely. The HeRep Mk II experienced a low of 8,734 counts at 15° and a high of 9,221 counts at 135°.

The HeRep Mk II was tested for its gamma-ray rejection capabilities while encased in the HDPE cylinder to better mimic real-world operational conditions. The gamma-ray measurement was performed with a 18 μg Cs-137 source at a distance of 5 cm from the front face of the moderator encasing the HeRep Mk II. A 10-minute measurement was performed for the source and background measurements. The HeRep Mk II reported 361 counts without a source present and 1337 counts with the Cs-137 source in place. Using the dimensions of the HeRep Mk II itself, without moderator, a solid-angle measurement was used to determine that the gamma-ray rejection ratio (GRR) was approximately $(7.60 \pm 0.43)\text{x}10^{-5}$ at 5 cm, when accounting for background. Including the dimensions of the HDPE moderator casing increases the GRR to $(2.19 \pm 0.12)\text{x}10^{-5}$.

5. Conclusions

The ^{3}He proportional counter had a net count rate of 17.13 ± 0.10 cps at 1 m from the aforementioned 54 ng bare ^{252}Cf neutron source. The HeRep device had a net count rate of 17.60 ± 0.10 cps at the same distance, amounting to $102.71 \pm 2.65\%$ of that of the Reuter Stokes ^{3}He proportional counter while inside of the HDPE moderator cylinder. Outside of the moderator, the ^{3}He tube had a count rate of 3.35 ± 0.05 cps and the HeRep device had a count rate of 3.19 ± 0.05, being $95.15 \pm 9.04\%$ of the ^{3}He proportional

Table 3
HeRep vs. ^{3}He-proportional counter with and without moderator

Detector	Measurement	Ct. Rate (cps)	% of He-3
HeRep	Moderated	17.60 ± 0.10	102.71 ± 2.65
HeRep	Bare	3.19 ± 0.05	95.15 ± 9.04
^{3}He Prop. Ctr.	Moderated	17.13 ± 0.10	–
^{3}He Prop. Ctr.	Bare	3.35 ± 0.05	–

counter, the results of which are listed in Table 3. The detection efficiency of the HeRep Mk II device is similar to a commercially available Reuter Stokes ^{3}He proportional counter of the same size pressurized to 4 atm. The high neutron detection efficiencies of the HeRep Mk II were achieved with a gamma-ray rejection ratio of approximately $2–7 \times 10^{-5}$. Higher efficiencies with the HeRep Mk II are possible by reducing the LLD, but an increase in gamma-ray sensitivity would be observed. The small angular dependence of the HeRep Mk II detection efficiency is a byproduct of the arrangement of the MSNDs within the cylindrical HeRep, however, the issue has shown to be mitigated with HDPE moderator around the device and would likely further decrease with the addition of internally-stored HDPE. Although the HeRep is presently a prototypical device, the projected cost of commercially available versions of the detector system are expected to fall between $1,500-$2,000 per unit. Furthermore, with higher efficiency MSNDs now under construction, the detection efficiency of next generation HeRep detectors should increase. The Helium Replacement (HeRep) neutron detector prototype has shown that a practicable replacement for aging ^{3}He-based proportional detectors can be developed using MSND-based technology.

Acknowledgments

Development of the He-Rep was funded by the Defense Threat Reduction Agency (DTRA), contract number HDTRA1-12-C-0004. The Electronics Design Laboratory (EDL) also played a crucial role in developing supporting electronics for the MSND technology and the development of the HeRep device. All microelectronic processing and fabrication of the MSNDs was performed in the Kansas State University S.M.A.R.T. Laboratory.

References

[1] D.S. McGregor, M.D. Hammig, Y.-H. Yang, H.K. Gersch, R.T. Klann, Design considerations for thin film coated semiconductor thermal neutron detectors-I: basics regarding alpha particle emitting neutron reactive films, Nucl. Instrum. Methods Phys. Res. A 500 (2003) 272–308.
[2] D.S. McGregor, J.K. Shultis, Spectral identification of thin-film-coated and solid-form semiconductor neutron detectors,, Nucl. Instrum. Methods Phys. Res. A 517 (2003) 180–188.
[3] T.C. Unruh, S.L. Bellinger, D.E. Huddleston, W.J. McNeil, E. Patterson, T.J. Sobering, D.S. McGregor, Design and operation of a 2-D thin-film semiconductor neutron detector array for use as a beamport monitor,, Nucl. Instrum. Methods Phys. Res. A 604 (2009) 150–153.
[4] J.K. Shultis, D.S. McGregor, Designs for micro-structured semiconductor neutron detectors, in *SPIE Hard X-ray, Gamma-ray, and Neutron Detector Physics X*, San Diego, CA USA, 2008.
[5] S.L. Bellinger, W.J. McNeil, T.C. Unruh, D.S. McGregor, Characteristics of 3D micro-structured semiconductor high efficiency neutron detectors,, IEEE Trans. Nucl. Sci. 56 (2009) 742–746.
[6] J.K. Shultis, D.S. McGregor, Design and performance considerations for perforated semiconductor thermal-neutron detectors,, Nucl. Instrum. Methods Phys. Res. A 606 (2009) 608–636.
[7] D.S. McGregor, W.J. McNeil, S.L. Bellinger, T.C. Unruh, J.K. Shultis, Microstructured semiconductor neutron detectors,, Nucl. Instrum. Methods Phys. Res. A 608 (2009) 125–131.
[8] S.L. Bellinger, W.J. McNeil, D.S. McGregor, Variant designs and characteristics of improved microstructured solid-state neutron detectors, in *IEEE Nuclear Science Symposium Conference Record*, Orlando, FL USA, 2009, pp. 986-989.
[9] C.M. Henderson, Q.M. Jahan, W.L. Dunn, J.K. Shultis, D.S. McGregor, Characterization of prototype perforated semiconductor neutron detectors,, Radiat. Phys. Chem. 79 (2010) 144–150.
[10] S.L. Bellinger, R.G. Fronk, W.J. McNeil, T.J. Sobering, D.S. McGregor, Enhanced variant designs and characteristics of the microstructured solid-state neutron detector,, Nucl. Instrum. Methods Phys. Res. A 652 (2011) 387–391.
[11] S.L. Bellinger, R.G. Fronk, W.J. McNeil, T.J. Sobering, D.S. McGregor, Improved high efficiency stacked microstructured neutron detectors backfilled with nanoparticle ^{6}LiF,, IEEE Trans. Nucl. Sci. 59 (2011) 167–173.
[12] D.S. McGregor, S.L. Bellinger, J.K. Shultis, Present status of microstructured semiconductor neutron detectors, J. Cryst. Growth 379 (2012) 99–110.
[13] M. Balzhauser, A. Dehoff, R. Engels, F. Hongesberg, J. Lauter, H. Leuth, M. Reetz, R. Reinartz, H.H. Richter, J. Schelten, T. Schmitz, A. Steffen, T. Vockenberg, Semiconductor diodes as neutron detectors for position-sensitive measurements and for application in personal neutron dosimetry, in *Neutrons in Research and Industry*, Crete, Greece, 1996.
[14] J. Schelten, M. Balzhauser, F. Hongesberg, R. Engels, R. Reinartz, A new neutron detector development based on silicon semiconductor and ^{6}LiF converter, Phys. B 234-236 (1997) 1084–1086.
[15] R.J. Nikolic, A.M. Conway, R. Radev, Q. Shao, L. Voss, T.F. Wang, J.R. Brewer, C.L. Cheung, L. Fabris, C.L. Britton, Nine element si-based pillar structured thermal neutron detector,, SPIE Hard X-ray, Gamma-ray, Neutron Detectro Phys. XII 7805 (2010).
[16] R.J. Nikolic, Q. Shao, L.F. Voss, A.M. Conway, R. Radev, T.F. Wang, M. Dar, N. Deo, C.L. Cheung, L. Fabris, C.L. Britton, M.N. Ericson, Si pillar structured thermal neutron detectors: fabrication challenges and performance expectations, in *SPIE Micro- and Nanotechnology Sensors, Systems, and Applications III*, 2011.
[17] S.L. Bellinger, R.G. Fronk, W.J. McNeil, J.K. Shultis, T.J. Sobering, D.S. McGregor, Characteristics of the stacked microstructured solid-state neutron detector, in *SPIE Hard X-ray, Gamma-ray, and Neutron Detector Physics XII*, San Diego, CA USA, 2010.
[18] S.L. Bellinger, R.G. Fronk, T.J. Sobering, D.S. McGregor, High-efficiency microstructured semiconductor neutron detectors that are arrayed, dual-integrated, and stacked, Appl. Radiat. Isotopes 79 (2012) 1121–1124.
[19] S.L. Bellinger, R.G. Fronk, W.J. McNeil, T.J. Sobering, D.S. McGregor, Improved high effiiciency stacked microstructured neutron detectors backfilled with nanoparticle ^{6}LiF, IEEE Trans. Nucl. Sci. 59 (2012) 167–173.
[20] Q. Jahan, E. Patterson, B. Rice, W.L. Dunn, D.S. McGregor, Neutron dosimeters employing high-efficiency perforated semiconductor detectors, Nucl. Instrum. Methods Phys. Res. B 263 (2007) 183–185.
[21] W.J. McNeil, S.L. Bellinger, T.C. Unruh, C.M. Henderson, P.B. Ugorowski, W.L. Dunn, R.D. Taylor, B.J. Blalock, C.L. Britton, Jr., D.S. Mcgregor, 1-D array of micro-structured neutron detectors, in *IEEE Nuclear Science Symposium*, Orlando, FL, USA, 2009, pp. 2008-11.
[22] S.L. Bellinger, R.G. Fronk, D.S. McGregor, T.J. Sobering, Arrayed high efficiency dual-integrated microstructured semiconductor neutron detectors, in *IEEE Nuclear Science Symposium*, Valencia, Spain, 2011, pp. 1281-1284.
[23] B.W. Cooper, S.L. Bellinger, A. Caruso, R.G. Fronk, W.H. Miller, T.M. Oakes, J.K. Shultis, T.J. Sobering, D.S. McGregor, Neutron energy spectrum with microstructured semiconductor neutron detectors, in *IEEE Nuclear Science Symposium*, Valencia, Spain, 2011, pp. 4783-4786.
[24] S.L. Bellinger, B.W. Cooper, N.R. Crawford, R.G. Fronk, T.J. Sobering, R.D. Taylor, D.S. McGregor, Very large area multi-element microstructured semiconductor neutron detector panel array, in *IEEE Nuclear Science Symposium*, Anaheim, CA USA, 2012, pp. 215-218.
[25] T.M. Oakes, S.L. Bellinger, W.H. Miller, E.R. Myers, R.G. Fronk, B.W. Cooper, T.J. Sobering, P.R. Scott, P. Ugorowski, D.S. McGregor, J.K. Shultis, A.N. Caruso, An accurate and portable solid state neutron rem meter,, Nucl. Instrum. Methods Phys. Res. A 719 (2013) 6–12.
[26] D.S. McGregor, J.K. Shultis, Reporting detection efficiency for semiconductor neutron detectors: a need for a standard, Nucl. Instrum. Methods Phys. Res. A 632 (2011) 167–174.
[27] S.R. Bolding, Design of a Neutron Spectrometer and Simulations of Neutorn Multiplicity Experiments with Nuclear Data Perturbations,, Masters of Science, Mechanical and Nuclear Engineering, Kansas State University, Manhattan, KS USA, 2013.
[28] S.L. Bellinger, R.G. Fronk, D.S. McGregor, Method of fabricating a neutron detector such as a microstructured semiconductor neutron detector, United States Patent 8778715, 2014.